Development and characterization of a 3D multicell microtissue culture model of airway smooth muscle

Adrian R. West, Nishat Zaman, Darren J. Cole, Matthew J. Walker, Wesley R. Legant, Thomas Boudou, Christopher S. Chen, John T. Favreau, Glenn R. Gaudette, Elizabeth A. Cowley and Geoffrey N. Maksym

Am J Physiol Lung Cell Mol Physiol 304:L4-L16, 2013. First published 2 November 2012;
doi: 10.1152/ajplung.00168.2012

Am J Physiol Lung Cell Mol Physiol 304: L4–L16, 2013.
First published November 2, 2012; doi:10.1152/ajplung.00168.2012.

CALL FOR PAPERS | *Bioengineering the Lung: Molecules, Materials, Matrix, Morphology, and Mechanics*

Development and characterization of a 3D multicell microtissue culture model of airway smooth muscle

Adrian R. West,[1] Nishat Zaman,[1] Darren J. Cole,[1] Matthew J. Walker,[1] Wesley R. Legant,[2] Thomas Boudou,[2] Christopher S. Chen,[2] John T. Favreau,[3] Glenn R. Gaudette,[3] Elizabeth A. Cowley,[4] and Geoffrey N. Maksym[1]

[1]*School of Biomedical Engineering, Dalhousie University, Halifax, Nova Scotia, Canada;* [2]*Department of Bioengineering, University of Pennsylvania, Philadelphia, Pennsylvania;* [3]*Department of Biomedical Engineering, Worcester Polytechnic Institute, Worcester, Massachusetts; and* [4]*Department of Physiology and Biophysics, Dalhousie University, Halifax, Nova Scotia, Canada*

Submitted 18 May 2012; accepted in final form 29 October 2012

West AR, Zaman N, Cole DJ, Walker MJ, Legant WR, Boudou T, Chen CS, Favreau JT, Gaudette GR, Cowley EA, Maksym GN. Development and characterization of a 3D multicell microtissue culture model of airway smooth muscle. *Am J Physiol Lung Cell Mol Physiol* 304: L4–L16, 2013. First published November 2, 2012; doi:10.1152/ajplung.00168.2012.—Airway smooth muscle (ASM) cellular and molecular biology is typically studied with single-cell cultures grown on flat 2D substrates. However, cells in vivo exist as part of complex 3D structures, and it is well established in other cell types that altering substrate geometry exerts potent effects on phenotype and function. These factors may be especially relevant to asthma, a disease characterized by structural remodeling of the airway wall, and highlights a need for more physiologically relevant models of ASM function. We utilized a tissue engineering platform known as microfabricated tissue gauges to develop a 3D culture model of ASM featuring arrays of ~0.4 mm long, ~350 cell "microtissues" capable of simultaneous contractile force measurement and cell-level microscopy. ASM-only microtissues generated baseline tension, exhibited strong cellular organization, and developed actin stress fibers, but lost structural integrity and dissociated from the cantilevers within 3 days. Addition of 3T3-fibroblasts dramatically improved survival times without affecting tension development or morphology. ASM-3T3 microtissues contracted similarly to ex vivo ASM, exhibiting reproducible responses to a range of contractile and relaxant agents. Compared with 2D cultures, microtissues demonstrated identical responses to acetylcholine and KCl, but not histamine, forskolin, or cytochalasin D, suggesting that contractility is regulated by substrate geometry. Microtissues represent a novel model for studying ASM, incorporating a physiological 3D structure, realistic mechanical environment, coculture of multiple cells types, and comparable contractile properties to existing models. This new model allows for rapid screening of biochemical and mechanical factors to provide insight into ASM dysfunction in asthma.

3D culture; tissue engineering; asthma; airway smooth muscle; airway wall remodeling

ASTHMA IS AN OBSTRUCTIVE AIRWAY disease characterized by increased airway resistance and hyperresponsiveness (AHR) to certain environmental stimuli. The primary cause of AHR is not clear but ultimately it is airway smooth muscle (ASM) contraction that is responsible for airway narrowing. Alterations in sensitivity, force generation, or shortening velocity of ASM in response to contractile agonists may be possible disease mechanisms. It is now also well established that asthma is characterized by airway wall remodeling, which includes thickening of the airway wall and increased ASM mass (52), altered extracellular matrix (ECM) composition (4, 19), infiltration of inflammatory cells (9), and epithelial dysfunction (33). Since airway wall remodeling may precede clinical symptoms (7), it is possible that a putative defect in ASM contractile function arises as a result of the remodeling process. Structural changes in the airway wall may manifest as altered mechanical loads that alter how ASM force development translates into airway narrowing. Such changes could also modulate ASM contractile phenotype through ECM signaling and mechanotransduction, but the relevance of these pathways to disease pathophysiology is poorly understood.

Because of the low availability of human asthmatic tissue suitable for ex vivo assessment of ASM contractile function, and to investigate key pathways under controlled conditions, many studies have attempted to simulate the biomechanical effects of airway wall remodeling by using normal cultured ASM cells or ex vivo tissue. For example, it has been consistently demonstrated in single cells and ex vivo ASM strips that ECM protein composition can modulate ASM proliferation, contractile protein expression, and contractile function (1, 17, 32). Similarly, collagenase digestion of ex vivo ASM strips (12) and precision-cut lung slices (39) increases apparent ASM contraction by acutely reducing the load that ECM stiffness presents to oppose contraction. However, these studies typically exhibit key methodological limitations. Although traditional 2D culture models permit full control over cell type and enable some control over substrate stiffness and composition, they nevertheless represent a nonphysiological mechanical environment. Thus potential interactions between ECM protein type, substrate stiffness, and 3D geometry are currently undefined. Also, although ex vivo models retain a more physiological 3D mechanical environment, the cell and matrix constitu-

Address for reprint requests and other correspondence: A. R. West, School of Biomedical Engineering, Dalhousie Univ., 5981 Univ. Ave., PO Box 15000, Halifax, NS, B3H 4R2, Canada (e-mail: a.west@dal.ca).

ency cannot be easily manipulated and the ability to recapitulate chronic remodeling events is somewhat limited.

3D culture models manufactured from in vitro cells with modern tissue engineering techniques present a more physiological environment than 2D cultures (26) and may be important for future applications to replace damaged lung tissue (54), but existing 3D models of ASM still present important limitations. Bulk gels and large ring structures consisting of human ASM embedded in collagen have been described (14, 42, 45). These systems allow for ASM contraction to be measured from gel shrinkage or in a myograph, respectively, but exhibit a low density of disorganized cells within the matrix and require excessive handling. More recently, fully engineered bronchioles have been developed to assess cell-cell signaling and ECM interactions. These bronchioles consist of a base layer of fibroblasts in a collagen matrix, internally lined with a layer of ASM cells and epithelium, and are maintained within a bioreactor that allows for simulated breathing (47). The ASM cells retain contractile protein expression, giving this system high physiological relevance; however, the mechanical loading for the ASM was undefined and contractile force was not measured. Furthermore, the long fabrication time of ~1 mo and resource intensive bioreactor design usually makes this system unattractive for routine usage. Thus a clear need remains to develop high-throughput in vitro models that focus on tissue biomechanics and ASM contractility.

The recent development of microfabricated tissue gauges shows great potential for assessing the contractile properties of cells in response to altered biomechanical environments (41). In the seminal study, polydimethylsiloxane (PDMS) substrates were produced containing an array of 80 wells, with each well containing a pair of flexible cantilevers spaced ~450 μm apart. A solution containing cells (3T3 fibroblasts) and monomeric ECM (collagen I) was introduced into the wells, the ECM polymerized, and the cells compacted and remodeled the ECM into a dense 3D microtissue around the top of the cantilevers. These 3T3 microtissues generated a baseline tension and exhibited tension changes in response to nonmuscle myosin activators and inhibitors.

In the present study, we utilized microfabricated tissue gauges to develop a 3D multicell microtissue culture model containing predominantly human ASM cells plus fibroblasts within a collagen I matrix, and we characterized its physiological properties. We assessed microtissue morphology, the dynamics of maximal contraction and tension ablation, long-term reproducibility of contractions, and response to a range of contractile and relaxant agents, and we compared microtissues to other ex vivo and in vitro models. Results indicate that ASM-3T3 microtissues behaved in a highly physiological manner and compare favorably to other models of ASM contraction and thus are a suitable platform for assessing modulation of ASM function in health and disease.

METHODS

Cell culture. Human ASM cells (*donor 12*) immortalized by stable transfection with human telomerase reverse transcriptase (hTERT; previously characterized in Ref. 25) were obtained as a generous gift from Dr. William Gerthoffer (University of South Alabama) and used for all key development and characterization of the model. Primary human ASM cells were obtained from macroscopically healthy tissue explants [approved by the Capital Health Research Ethics Board (Halifax, Nova Scotia, Canada)] as described previously (22) and used at passage 3–4. Green fluorescent protein (GFP)-labeled NIH-3T3 cells and WI-38 human lung fibroblasts were purchased commercially (CellBioLabs AKR-214 and ATCC CCL-75, respectively) and unlabeled NIH-3T3 were obtained as a generous gift from Dr. Neale Ridgway (Dalhousie University). All cells were maintained in feeder medium consisting of DMEM/F12 (Invitrogen 11330) with 10% FBS (Invitrogen 12483) and 1% penicillin-streptomycin (Invitrogen 15140) in a 37°C humidified incubator with 5% CO_2.

Microtissue fabrication. Microfabricated tissue gauges (substrates) with stiff and flexible cantilevers were produced and characterized as described previously (41). Substrates were sterilized by filling with 70% ethanol and placing under UV light for 15 min, then air dried. The PDMS was surface treated with 0.2% Pluronic F-127 (Invitrogen P6866) for 2 min to reduce cell adhesion, rinsed once with PBS, and air dried. A medium-collagen mixture was made from concentrated solutions to obtain a final concentration of 1 × DMEM/F12 (Invitrogen 12400), 14.3 mM $NaHCO_3$, 15 mM D-ribose (Sigma R9629), 1% FBS, 2.5 mg/ml collagen I (BD Biosciences 354326) plus 1 M NaOH to achieve a final pH of 7.0–7.4. This solution was added to the substrates, pipetted into the wells, and degassed for >5 min to remove air bubbles around the cantilevers. Trypsinized and pelleted cells (5×10^5; 100% ASM or 80% ASM plus 20% fibroblasts, see details of individual experiments in RESULTS) were resuspended in the medium-collagen mixture and added to the substrates before centrifuging for 90 s at 300 × relative centrifugal force (RCF) in an IEC Centra MP4R with swinging bucket rotor 224. Excess collagen and cells were aspirated and removed with a cell scraper before incubating at 37°C for 15 min to initiate collagen polymerization. An additional 5×10^5 cells (same cell mix as used in previous centrifugation step) suspended in feeder medium was added to the substrate and centrifuged for 45 s at 300 × RCF before incubating at 37°C for 10 min to allow for cell adherence. Excess cells were gently washed from the surface of the PDMS with PBS, leaving a layer of cells on top of the polymerized collagen. Feeder medium was added to the substrates and changed after 24 h, and all microtissues were used for experimentation at 3–4 days.

Imaging and histology. Imaging of live and fixed microtissues was performed on a Leica DM IRB microscope with a ×10 or ×20 lens, and images were captured with a PCO Sensicam CCD camera with custom software [Beadtracker (22)]. Images were uniformly adjusted for brightness and contrast only, ensuring that no details were obscured. Fixation was performed as described previously (55), with modifications. In brief, microtissues were rinsed with cytoskeleton buffer (CB), fixed with 4% paraformaldehyde in CB for 20 min, then permeabilized with 0.3% Triton X-100 and 4% paraformaldehyde in CB for 10 min. Cell were washed with CB and stored in CB-TBS at 4°C prior to staining. Nuclei were stained with DAPI (Invitrogen D1306, 0.4 μg/ml, fixed cells) or Hoechst 33342 (Invitrogen H1399, 5 μg/ml, live cells) in PBS for 30 min, and actin filaments were stained with 1 U phalloidin-AF488 (Invitrogen A12379) for 1 h. Rabbit anti-MHC (Santa Cruz sc-20641, 1:100) and donkey anti-rabbit AF488 (Invitrogen A21206, 1:200) were used for 1 h each to stain for myosin heavy chain (MHC).

Tension measurement and manipulation. The medium on microtissues was exchanged to serum-free insulin-transferrin (IT) medium consisting of DMEM/F12 with 5.8 μg/ml insulin (Sigma I1882) and 1.0 μg/ml transferrin (Sigma T4382) prior to all tension measurement and manipulation experiments. Up to eight representative mechanically secure microtissues were selected from each substrate, and images were taken for baseline tension. Maximal drug doses (isotonic 80 mM KCl, 100 μM histamine, 100 μM acetylcholine, 100 μM forskolin, 10 μM cytochalasin D) were prepared in IT medium and added to all of the microtissues on a substrate, with images taken at various time points depending on the specific experiment. Where microtissues received multiple successive treatments, drugs were administered in an order that did not generate any signaling pathway

interference. After the final drug treatment, microtissues were disrupted by sonication and vigorous pipetting, and the wells were imaged again to determine unloaded cantilever distances. Substrates were recycled by treating with crude collagenase (Sigma C0130) in IT medium plus 5 mM $CaCl_2$ and then TrypLE Express (Invitrogen 12604) to remove ECM proteins, rinsed with distilled water, and air dried.

The (x,y) centroid of both cantilevers in each unloaded, baseline, and drug-treated image was determined by manually tracing around the top of the cantilevers with ImageJ 1.44, and the pixel distance between cantilevers was converted to a micrometer (μm) distance by using a conversion factor obtained with a graticule. Microtissue tension in each baseline and drug-treated image was then calculated by subtracting the distance from the unloaded cantilever distance and applying the spring constants for stiff (k = 0.397 μN/μm) and flexible cantilevers (k = 0.098 μN/μm) as described previously (41). Deflections were considered linear up to 30 μm per cantilever (11) (tension = 23.8 and 5.9 μN for stiff and flexible cantilevers, respectively), with a maximum practical measurement limit of 45 μm per cantilever (tension ~35.7 and 8.8 μN).

Strain mapping. Regional displacements were estimated across the microtissue by using High Density Mapper software as described previously (8). In brief, a region of interest (ROI) ~715 × 355 pixels in size was selected that encompassed the microtissue between the cantilevers, and the ROI was then divided into 32 × 32 pixel subimages. These subimages were then compared on a frame-to-frame basis with a phase correlation algorithm with subpixel detection, resulting in a subimage displacement accuracy of ± 0.05 μm (38). The resulting displacements were used to calculate strain maps by using custom code written with MATLAB (MathWorks, Natick, MA). Strain was approximated in the x (horizontal) direction by calculating the linear slope of displacements across five adjacent subimages.

Two-dimensional drug testing. Petri dishes (35 mm) were coated with 100 μg/ml collagen I in PBS for 1 h and then rinsed with PBS. ASM cells were seeded in the dishes at 1×10^4 cells/cm^2 in feeder medium, maintained until they were >90% confluent, and transferred to IT medium 24 h prior to use. Optical magnetic twisting cytometry (OMTC) was performed as described previously (18), with modifications. In brief, cells were washed with IT medium before adding RGD-peptide-coated ~4.5 μm ferromagnetic beads to the center of the dish, and incubated at 37°C for 20 min. Excess beads were removed by washing with IT medium, and incubated for a further 20 min. Petri dishes were placed on the microscope, magnetized twice, and twisted in an oscillating magnetic field with 2-A coil current that applied 91.8-Pa specific torque to the beads to collect baseline stiffness data (21). Drug solutions were added to the dish, gently mixed, and incubated for 3 min, before beads were magnetized once and postdrug stiffness data were collected. Cytoskeletal stiffness (G′, Pa/nm) was calculated from the bead displacement and applied torque by use of custom MATLAB code (22), and the median value for each field was used to determine the percent change from baseline values. Stiffness changes measured by this method are directly proportional to the net contractile moment measured by traction force microscopy (60).

Gene expression analysis by qPCR. Gene expression analysis of key contractile/regulatory proteins, transcription factors, and candidate housekeeping controls was performed as described previously, with modifications (61). In brief, ASM-3T3 microtissues and 2D ASM cells were seeded as described above and maintained in feeder medium for 2 days. Dissociated microtissues and cells growing on the surface of the PDMS were manually removed from microtissue substrates by pipetting. Total RNA was isolated from microtissues and petri dishes by using the Qiagen RNeasy Mini Kit, before concentration and purity of the RNA were assessed by A_{260}:A_{280} spectrophotometry. Reverse transcription was performed with 0.75 μg total RNA by use of the Qiagen QuantiTect Reverse Transcription Kit. cDNA equivalent to 30 ng of total RNA was then amplified in duplicate by use of the Qiagen QuantiTect SYBR Green PCR Kit and 300 nM of the appropriate primers (Table 1) in a Stratagene Mx3000P thermal cycler. Cycling conditions involved an initial 15-min incubation at 95°C for Taq activation, followed by 45 cycles of denaturing at 95°C for 15 s, annealing at 56°C for 30 s, and extension at 72°C for 40 s. Crossing thresholds (Ct) were determined by using the Stratagene MxPro v3.20 software, and the most stable housekeeping control was selected by using Ct input for Bestkeeper (53) and $E^{\Delta Ct}$ input for NormFinder (3). Relative gene expression was calculated by efficiency-corrected ΔΔCt and the final data were normalized such that the condition with the highest expression presented a mean result of 1 AU.

Data analysis and statistics. All numerical data are presented as means ± SE. Statistical tests as described in the results were performed with the Analyse-It 2.26 software package, with $P < 0.05$ considered statistically significant.

RESULTS

ASM-only microtissues. One-day-old ASM-only microtissues produced on substrates with flexible and stiff cantilevers are shown in Fig. 1, *A* and *B*, and inward deflection of the cantilevers from the development of baseline tension is evident with both cantilever stiffnesses. However, the excessive deflection of the flexible cantilevers greatly exceeded the point where cantilever bending responses were linear and accurate force measurements were not possible; thus all further experiments were performed on substrates with stiff cantilevers. The gross morphology of ASM-only microtissues observed with bright-field imaging demonstrated an organized structure with

Table 1. *Primers used for qPCR gene expression analysis*

Gene Common Name (code)	Forward Primer	Reverse Primer	Accession No. (amplicon location)
Smooth muscle myosin heavy chain (MYH11/MHC)	5′-CTGCAGAGACAGCTTCACGA-3′	5′-CTCCCCTTGATGGCAGAGTC-3′	NM_002474.2 (4887–5026)
Myosin light chain kinase (MYLK)	5′-GCCAGGAGGCTGGAGAATGCG-3′	5′-CCACATGTCTGTGGCGTAGCCG-3′	NM_053025.3 (5107–5217)
Myosin phosphatase target subunit 1 (MYPT1)	5′-TGCTGCAGCTTCTACCACAACCC-3′	5′-TGAGGTATGATCTGCGTCTCTCCCT-3′	NM_002480.2 (2187–2278)
Serum response factor (SRF)	5′-AGCTCCACCAGATGGCTGTGATAG-3′	5′-ACTCTTGGTGCTGTGGGCGGT-3′	NM_003131.2 (1896–1996)
Myocardin (MYOCD)	5′-GCACTGCACAGAACTCAGGAGCAC-3′	5′-GGCTCCAGAGAAGGGCGGGT-3′	NM_001146312.1 (2347–2435)
Phospholipase A2 (YWHAZ)	5′-CGCTGGTGATGACAAGAAAGGGAT-3′	5′-GGGCCAGACCCAGTCTGATAGGA-3′	NM_003406.3 (537–652)
Ubiquitin C (UBC)	5′-ATAAGGACGCGCCGGGTGTG-3′	5′-GCATTGTCAAGTGACGATCACAGCG-3′	NM_021009.5 (364–462)
Glyceraldehyde-3-phosphate dehydrogenase (GAPDH)	5′-CTGCTGATGCCCCCATGTTCGT-3′	5′-TGGTGCAGGAGGCATTGCTGATG-3′	NM_002046.4 (548–634)

Primers were selected by using Primer-BLAST (http://www.ncbi.nlm.nih.gov/tools/primer-blast/) to span exon-exon junctions to prevent amplification of genomic DNA, with specificity checked against the *Mus musculus* RefSeq mRNA database to ensure that equivalent targets from 3T3 cells would not be coamplified. Primer specificity was initially assessed by agarose gel electrophoresis and continually assessed by melting curve analysis.

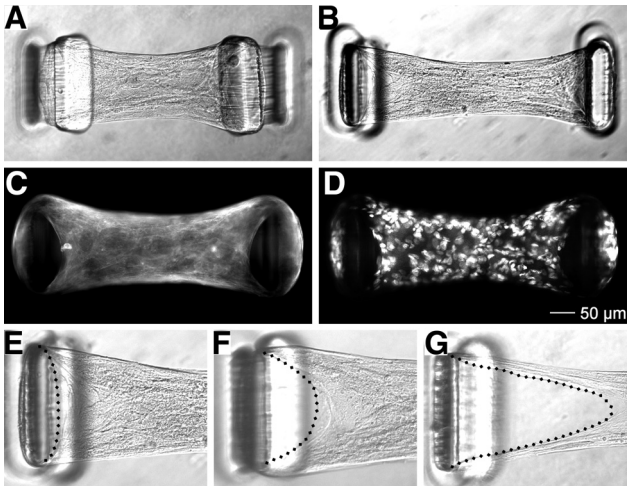

Fig. 1. Airway smooth muscle (ASM)-only microtissues. ASM-only microtissues produced on substrates with flexible (*A*) and stiff cantilevers (*B*) exhibit cantilever deflection, indicating tension development. Epifluorescence imaging for F-actin (*C*) and nuclei (*D*) shows a homogenous 3D structure that was highly organized, including the development of actin stress fibers. However, ASM-only microtissues exhibited poor structural integrity (*E–G*), progressively dissociating from the tops of the cantilevers (dashed lines) before ultimately failing in less than 3 days.

visible alignment of cell bodies parallel to the direction of tension development. Staining for filamentous actin (Fig. 1*C*) showed the formation of stress fibers that encircled the outside of each cantilever and radiated inward toward the center of the microtissue. Qualitatively, nuclei were evenly distributed throughout the microtissue along all axes, indicating the formation of a true 3D structure (Fig. 1*D*).

Despite the high degree of cellular alignment reminiscent of that observed in vivo, ASM-only microtissues proceeded to exhibit poor structural integrity over time. In all cases ASM-only microtissues progressively pulled away from the top of the cantilevers before dissociating completely, often remaining attached to just one cantilever (Fig. 1, *E–G*). Tissue dissociation became apparent within 24 h after fabrication with a 100% tissue failure rate observed at 3 days. This was deemed insufficient stability for many functional assessments and made observing phenotypic changes in ASM cells impossible; thus ASM-only microtissues were not characterized further.

ASM-3T3 microtissues. Since 3T3 microtissues previously exhibited no structural problems (41), we created multicell microtissues comprised of both ASM and 3T3 cells, which increased structural integrity dramatically. Inclusion of 3T3 cells at 20% of the total cell content was used for this study since it was the lowest concentration of fibroblasts that offered tangible benefits, with survival rates of ASM-3T3 microtissues as high as 50% at 7 days. Despite the substantial improvements in survival time, the primary mode of ASM-3T3 microtissue failure was similar to ASM-alone tissues, i.e., progressively dissociating from the cantilevers. Of the microtissues that remained after very long time periods (>10 days), cellular organization visibly deteriorated; the microtissues lost their aligned appearance with an increased appearance of rounded cells throughout the tissue, decreases in baseline tension became evident, and the microtissues progressively decreased in volume (data not shown). This apparent loss of cells coincided with an increased number of cells growing on the floor of the microtissue wells, suggesting that over these long time periods cells migrated out of the microtissue. Nevertheless, at earlier time points gross morphology and early tension development of ASM-3T3 microtissues was not different from that seen with ASM cells alone and presented a consistently stable period of study for at least 5 days; thus ASM-3T3 microtissues were used for all subsequent experiments at 3–4 days.

ASM-3T3 microtissues were fabricated with GFP-labeled 3T3 fibroblasts in a subset of experiments to demonstrate microtissue formation and baseline tension development, and to determine the spatial distribution of fibroblasts (Fig. 2). After seeding, ASM-3T3 microtissues compacted rapidly, completely pulling the collagen gel away from the sides of the wells within 6 h and coalescing into dense tissues. Tension development was apparent at 6 h and increased steadily up to 48 h. The 3T3 fibroblasts were evenly distributed within the microtissues at each time point and showed no selective migration toward or away from the cantilevers, and the relative proportion of ASM to GFP-3T3 in the tissue did not appear to change over time. This is in stark contrast to the same cells grown together on traditional 2D substrates; the faster proliferating 3T3 cells rapidly take over the culture, and in areas where ASM cells continue to be present at a high density they form as distinct colonies that do not integrate with the 3T3 cells (data not shown).

Epifluorescence images of 2- to 3-day-old ASM-3T3 microtissues are shown in Fig. 3. ASM-3T3 microtissues were highly

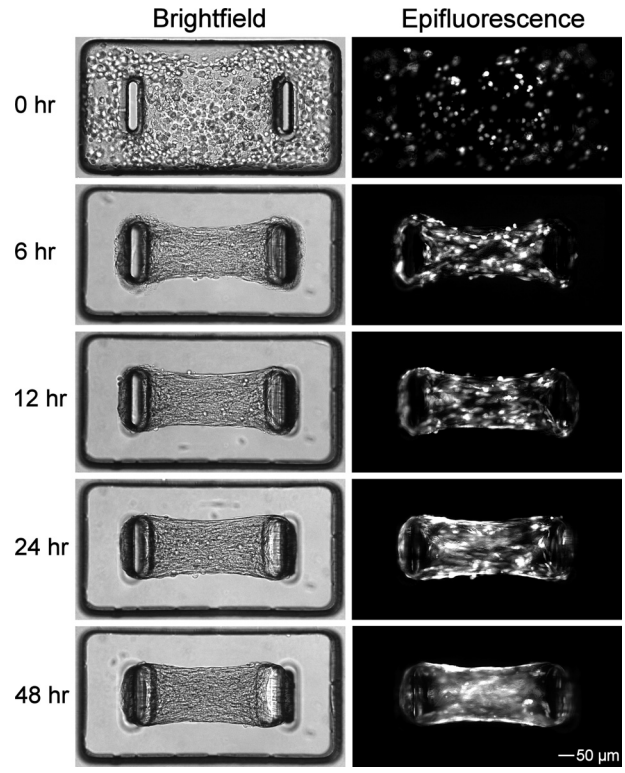

Fig. 2. ASM-3T3 microtissue formation. Temporal formation of ASM-3T3 microtissues was demonstrated by use of green fluorescent protein (GFP)-labeled 3T3 cells. Bright-field imaging shows that microtissue compaction and gel remodeling was largely complete at 6 h, whereas baseline tension development continued steadily up to 48 h. Epifluorescence imaging for GFP demonstrates that 3T3 cells are evenly distributed throughout the microtissue at all time points.

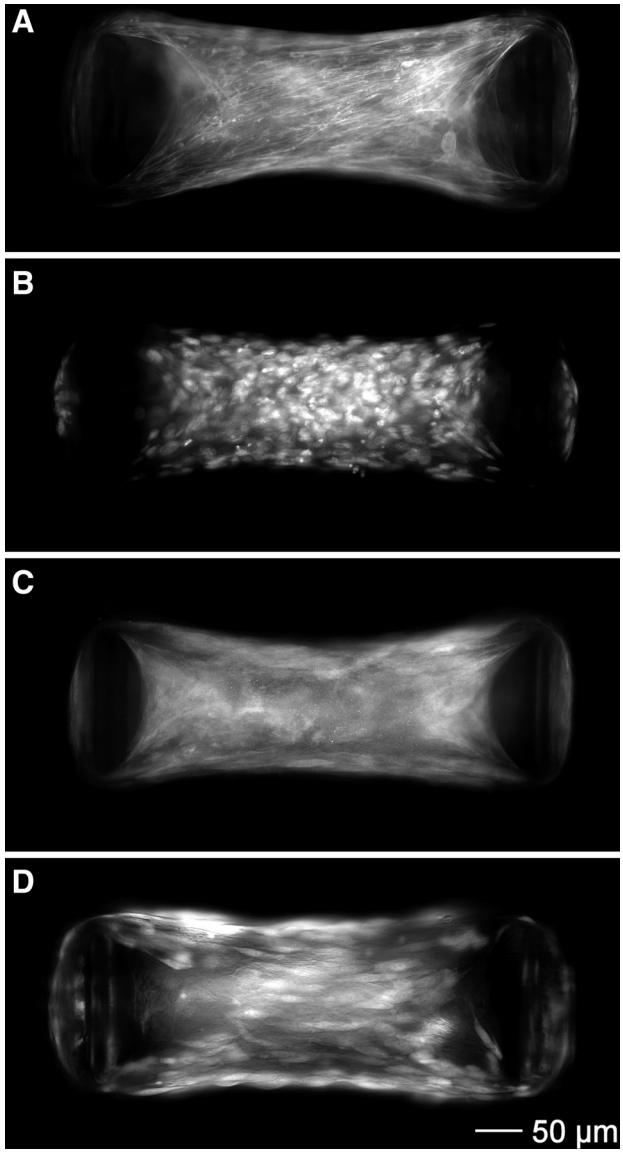

Fig. 3. ASM-3T3 microtissue histology. ASM-3T3 microtissues exhibited a high degree of structural organization including the development of actin stress fibers (*A*) and cell nuclei qualitatively distributed evenly in 3D (*B*). Myosin heavy chain (MHC) staining was present, but diffuse (*C*). High-magnification images of microtissues containing GFP-3T3 fibroblasts demonstrated that the cell bodies line up parallel with the direction of tension development (*D*).

organized and morphologically similar to ASM-only microtissues, with actin stress fibers that encircled the cantilevers, radiated inward toward the center of the microtissue and aligned parallel to the direction of tension (Fig. 3*A*). Nuclei were qualitatively present throughout a wide *z*-axis range, both above and below the focal point, indicating the formation of a true 3D structure (Fig. 3*B*). MHC staining was much more diffuse than for F-actin, exhibiting only small areas of high-density staining near the cantilevers that may indicate thick filament formation (Fig. 3*C*). Considering that these microtissues were not in a contracted state, this observation is consistent with MHC organization seen in resting ex vivo smooth muscle (23). Images of microtissues containing GFP-3T3 show that the cell bodies line up parallel to the direction of tension development, and the wide *z*-axis distribution further demonstrates that fibroblasts are distributed evenly within the 3D structure (Fig. 3*D*).

Induced tension development and ablation. To observe the dynamics of induced tension development and ablation, we exposed ASM-3T3 microtissues to KCl for 20 min to induce maximal ASM contraction, followed immediately by 20-min treatment with cytochalasin D to disrupt the actin cytoskeleton. The results from a single typical microtissue imaged at 15-s intervals are shown in Fig. 4, *A–D* and Supplemental Video S1 (Supplemental Material for this article is available online at the Journal website), starting from baseline microtissue length and tension of 445 μm and 14.3 μN, respectively (Fig. 4*B*). The contraction phase was characterized by a steady shortening of the microtissue to a final length of 414 μm (7.0% decrease), resulting in an 82% increase in tension (26.9 μN) (Fig. 4*C*). Cytoskeletal disruption resulted in a quasi-biphasic response, with a very high lengthening rate during the first ~5 min, followed by a long period of slow continual lengthening. Microtissue length ultimately increased above baseline levels to 462 μm (3.8% increase), representing a 45% decrease in tension below baseline levels (7.9 μN) (Fig. 4*D*). Microtissues also narrowed marginally along the *y*-axis during contraction and broadened during relaxation.

Contractile reproducibility. The robustness of the model and temporal reproducibility of results were determined by subjecting ASM-3T3 microtissues ($n = 23$) to a series of maximal contractions involving a 20-min exposure to KCl, followed by a 30-min washout period. The protocol was repeated six times within 5.5 h, with tension recorded at the start and end of each contraction phase and normalized to the first baseline reading (Fig. 4*E*). Tension development from the first contraction was modestly but significantly higher than the second contraction (paired *t*-test $P < 0.0001$), but each subsequent contraction was not different from the second (paired *t*-tests $P \geq 0.2912$). Baseline tension was remarkably consistent, returning to the same level after each washout (repeated-measures one-way ANOVA $P = 0.2545$). None of the measured microtissues exhibited any qualitative decrease in structural integrity during the course of this experiment.

Strain mapping. To determine the spatial and temporal distribution of tension changes, *x*-axis strain from the microtissue in Fig. 4, *A–D* was mapped over 15-s intervals at 1, 5, and 10 min during both contraction and relaxation (Fig. 5*A*). Qualitatively, the rate of contraction was not randomly distributed but was fairly uniform throughout the microtissue, displaying little spatial heterogeneity at 1 min with an isolated area of faster contraction near the center-right of the tissue at the latter time points. In contrast, tension changes following cytoskeletal disruption exhibited high spatial and temporal variability. At 1 min when the tissue was lengthening rapidly, high strain rates were heavily localized to the ends of the tissue near the cantilevers. From 5 min onward, strain was more apparent in the center of the microtissue than at the ends. The distribution of strain was not Gaussian (D'Agostino-Pearson K^2 $P < 0.0001$) but exhibited a mostly symmetric long-tailed distribution in all cases except for relaxation at 1 min, which was strongly positively skewed, i.e., higher strain rates in some regions (Fig. 5*B* and Table 2).

Physiological responses. The physiological function of key contractile and relaxation pathways in ASM-3T3 microtissues was determined by recording tension values at baseline and in

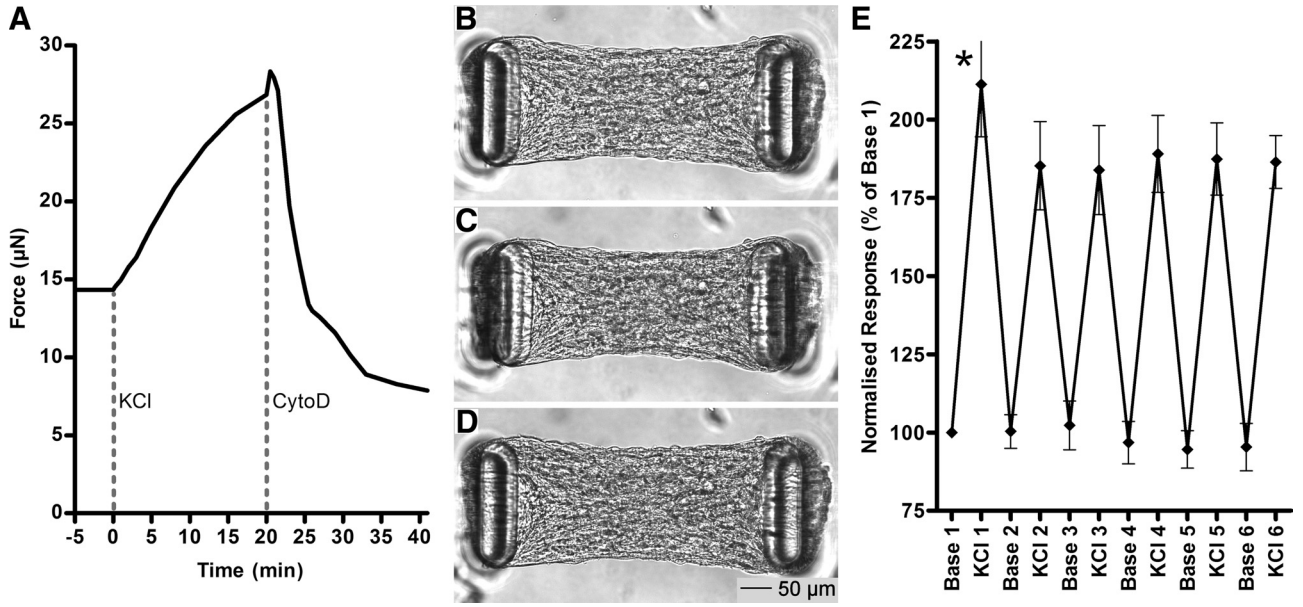

Fig. 4. Tension manipulation and reproducibility. Addition of KCl to microtissues induced contraction of ASM cells, resulting in a gradual increase in tension, whereas disruption of the actin cytoskeleton with cytochalasin D resulted in a sudden and dramatic relaxation with tension ending well below baseline levels. The time course for a single typical example is shown in *A*. The small jump in tension at 20 min is an imaging artifact during drug addition. Bright-field images at baseline (*B*) and at the peak response to KCl (*C*) and cytochalasin D (*D*) show the full range of length and shape changes that occurred in this microtissue. *E*: repeated KCl contraction (20 min) and washout (30 min) cycles on multiple ASM-3T3 microtissues ($n = 23$) show that the first contraction on a given microtissue was modestly but significantly higher than the second (paired *t*-test $P < 0.0001$), but subsequent contracted and baseline tension levels were highly reproducible (NS).

response to a 10-min exposure to a range of contractile and relaxant agents (Fig. 6*A*). ASM-3T3 microtissues ($n \geq 31$) responded to all drugs tested (1-way ANOVA $P < 0.0001$); maximal doses of histamine and acetylcholine both gave an equivalent mild contractile response, increasing tension to 37 and 40% above baseline levels, respectively. KCl caused a much stronger contractile response, approximately twice that of histamine, increasing tension 75% above baseline. Interestingly, the ASM relaxant forskolin was able to reverse the contraction to KCl, and also further reduce tension to 32% below baseline levels, demonstrating that there is a significant level of actinomyosin cross-bridge activation even in resting microtissues. The high degree of tension loss to cytochalasin D (>60% below baseline levels) strongly indicates that the majority of baseline tension is generated by active processes within the cells, with low passive tension contribution from the collagen ECM.

To demonstrate the utility of microtissues to examine lung cell function in a more physiologically relevant context, microtissues were also fabricated using primary human ASM cells from multiple donors in combination with 3T3 fibroblasts (1°ASM-3T3) and WI38 human lung fibroblasts (1°ASM-WI38). Survival of microtissues with each different cell combination was equivalent. Baseline tension of both 1°ASM microtissue types was higher than for immortalized cells, and 1°ASM microtissues contracted to acetylcholine and KCl (1-way ANOVA $P \leq 0.0003$; Fig. 6*B*) and demonstrated significant tension reductions in response to forskolin and cytochalasin D (data not shown). Interestingly, no differences were observed between the results from the two different fibroblast types.

Comparison to ex vivo tissue. To compare the force developed by microtissues to measurements from ex vivo ASM strips, we computed tissue stress from the tension normalized to cross-sectional area. Microtissue cross-sectional area at the tissue center was first measured by fixing a group of microtissues and excising the wells from the substrate to take top-down and side-on images. Microtissue height and width were measured with a calibrated scale and area was calculated as 0.0135 ± 0.0007 mm^2 ($n = 7$) assuming an oval shape. Using the peak tension generated by 10-min KCl contractions (0.0202 mN and 0.0279 mN for ASM-3T3 and 1°ASM-3T3, respectively) yielded mean stress values of 1.50–2.07 mN/mm^2. Comparing with other reported contracted stress values [35.1 mN/mm^2 for canine bronchial smooth muscle (BSM) (35), 29.4 mN/mm^2 for human BSM (13), 16.2 mN/mm^2 for Fischer rat tracheal smooth muscle (10)], ASM-3T3 microtissues generated ~8- to 23-fold lower stress than freshly excised ex vivo ASM strips.

Comparison to in vitro models. To evaluate ASM-3T3 contractile force development against other in vitro models, we first compared the overall tension per cell with a previous study using 3T3 fibroblasts alone (41). Nuclei in ASM-3T3 microtissues were counted by live-cell imaging at multiple focal lengths and found to contain 370 ± 3.8 ($n = 40$) cells, before microtissues were treated with acetylcholine, KCl, and forskolin, and tension per cell was calculated. Compared with the same metric measured in 3T3-only microtissues produced with cantilevers of the same stiffness, ASM-3T3 microtissues generated higher baseline tension per cell, and substantially more tension when contractile activation to acetylcholine and KCl is considered (Fig. 7*A*) (*t*-test $P < 0.0001$). Interestingly, microtissues that were relaxed with forskolin, representing the cytoskeletal tension of ASM cells without contribution from the contractile apparatus, produce 26.9 ± 2.0 nN/cell; this is not significantly different from the 24 nN/cell produced by 3T3 cells alone (*t*-test $P = 0.1791$).

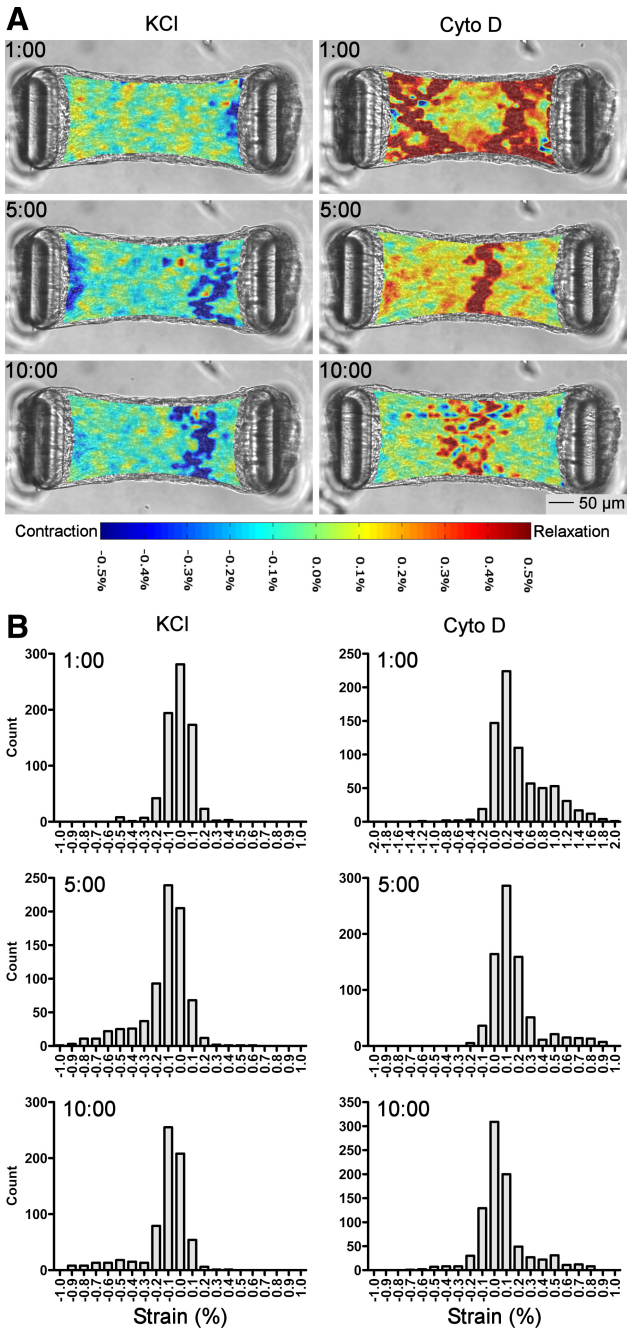

Fig. 5. Strain distribution during tension manipulation. *A*: maps of *x*-axis strain calculated over 15-s intervals during contraction to KCl displayed little spatial and temporal heterogeneity. However, tension ablation to cytochalasin D was heavily localized to the areas near the cantilevers at 1 min but was predominantly in the center of the tissue at later time points. *B*: histograms show that strain was not normally distributed but was largely symmetric around the median with long tails; axis scales are set to maximize tail visibility. See Table 2 for summary statistics.

A second in vitro comparison was performed by OMTC measurements of cell stiffness for the same ASM cells grown on traditional 2D cell culture substrates in response to the contractile and relaxant agents. Microtissue tension data from Fig. 6 and OMTC stiffness data were both normalized to their respective baselines and are shown in Fig. 7*B*. Surprisingly, acetylcholine and KCl gave virtually identical normalized contractile responses (*t*-test $P = 0.5533$ and 0.8173, respectively). In stark contrast, histamine responses in 2D cells were significantly higher than those in 3D microtissues (*t*-test $P < 0.0001$). The relaxation response to forskolin and the response to cytoskeletal disruption by cytochalasin D were also modestly but significantly higher in 3D than the same cells in 2D (*t*-test $P = 0.0046$ and 0.0399, respectively).

Gene expression analysis. Contractile phenotype of ASM-3T3 microtissues was compared with 2D cell cultures by gene expression analysis. Table 3 shows that expression of candidate housekeeping controls YWHAZ, UBC, and GAPDH was consistently three- to fourfold lower in 3D microtissues than in 2D cells (*t*-test $P < 0.0001$). Nevertheless, all three genes were strongly correlated with the Bestkeeper index (53), and UBC was ultimately selected as a suitable reference gene for ΔΔCt calculations because of its high stability in NormFinder analysis (3). Importantly, gene expression for key contractile/regulatory proteins and transcription factors was regulated by substrate geometry (Fig. 7*C*); 3D microtissues had higher expression of MHC (6.5-fold higher, *t*-test $P = 0.0233$), MYLK (13.4-fold higher, *t*-test $P < 0.0001$) and MYOCD (2.3-fold higher, *t*-test $P = 0.0107$), whereas SRF expression decreased 1.5-fold (*t*-test $P = 0.0056$) and MYPT1 expression was not significantly different (*t*-test $P = 0.4973$).

DISCUSSION

Existing in vitro and ex vivo models of ASM contractile function have been able to demonstrate the importance of the ECM environment and mechanical loads that oppose ASM contraction (1, 12, 17, 32, 39), but these approaches have methodological limitations that prevent them from replicating the full gamut of biomechanical changes thought to occur in asthma. Specifically, traditional 2D culture techniques present a nonphysiological mechanical environment, whereas the ability of ex vivo tissue to recapitulate chronic remodeling events is somewhat limited. Tissue engineering approaches are attractive because of their broad range of potential applications (54) and models such as microfabricated tissue gauges can circumvent many existing limitations by creating 3D cultures that allow for direct assessment of cellular tension, a tunable auxotonic load for cells to contract against and an easily modifiable extracellular matrix (11, 41). In the present study we utilized microfabricated tissue gauges to develop a 3D multicell microtissue culture model of ASM and characterized important morphological and contractile properties. Crucially,

Table 2. *Summary statistics for strain*

	Mean strain over 15 s ($n \geq 692$ subimages)	Standard Deviation	D'Agostino-Pearson K^2 Normality Test
Contraction 1:00	−0.015%	0.110%	$P < 0.0001$
Contraction 5:00	−0.130%	0.207%	$P < 0.0001$
Contraction 10:00	−0.120%	0.196%	$P < 0.0001$
Relaxation 1:00	0.407%	0.442%	$P < 0.0001$
Relaxation 5:00	0.155%	0.190%	$P < 0.0001$
Relaxation 10:00	0.064%	0.206%	$P < 0.0001$

Microtissue strain determined over 15-s intervals displayed little heterogeneity during contraction to KCl at all time points. In contrast, strain rate was highly variable at the 1 min mark of relaxation but was largely homogeneous at 5 min onward. Strain data were not normally distributed but were heavily centred around the median with long tails. See Fig. 5*A* for strain maps and Fig. 5*B* for histograms.

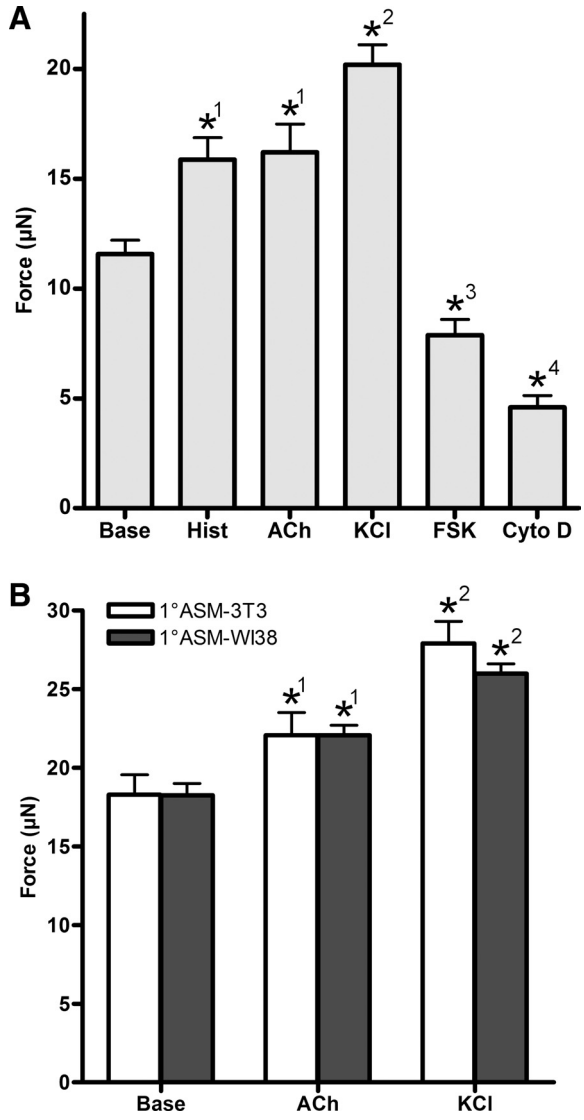

Fig. 6. Physiological drug testing. *A*: ASM-3T3 microtissues ($n \geq 31$) exhibited mild contractile responses to both histamine and acetylcholine but a substantially stronger response to KCl. Forskolin relaxed microtissues below baseline levels, whereas cytochalasin D ablated 60% of baseline tension. *B*: 1°ASM-3T3 ($n = 8$) and 1°ASM-WI38 ($n = 16$) microtissues both had a higher baseline and contracted tension values than microtissues with hTERT ASM cells, but no difference was seen between the 2 different fibroblast types. *Significant difference from baseline; groups with the same superscript number in each panel are not significantly different (1-way ANOVA with Tukey's posttest). Base, baseline; Hist, histamine 100 μM; ACh, acetylcholine 100 μM; KCl, 80 mM; FSK, forskolin 100 μM; Cyto D, cytochalasin D 10 μM.

we demonstrated that ASM cells in microfabricated tissue gauges were able to compact and remodel a polymerized collagen I gel, self-assemble into dense microtissues around the top of the cantilevers, and generate baseline tension. ASM microtissues displayed many essential features consistent with a highly organized 3D structure, including a qualitatively even distribution of nuclei along all axes and the formation of actin stress fibers parallel to the direction of tension formation, and in situ assessment of contractile force. These features represent a marked improvement on existing 3D models of ASM in bulk gels and ring structures where cells display poor organization, require excessive handling to mount the construct in a myograph, and do not present an appropriate mechanical load opposing contraction (14, 42, 45, 47).

Microtissue contractile function. ASM-3T3 microtissues responded appropriately to a number of key contractile (histamine, acetylcholine, and membrane depolarization) and relaxant (forskolin and cytochalasin D) stimuli and displayed many features essential to a physiological model of ASM contraction. The time course of tension development and ablation was similar to that observed with ex vivo ASM, and tissues were very consistent in their contractile responses after an initial KCl contraction. The modest decrease in force development after the initial contraction may be due to some adaptation within the cells or tissue, or possibly mechanical slipping at the cantilevers, but this is not known. Importantly, strain was largely homogeneously distributed across the microtissue during contraction and relaxation. Although the strain distribution was not Gaussian it was more heavily centered around the median, with longer symmetric tails than seen for the log-normal distribution of stiffness and contractility of cells measured in 2D culture by OMTC (21). To develop such consistent strain patterns in 3D, tension must be generated relatively evenly throughout the tissue; either cells adapted to have similar stiffness and contractility, or this indicates that the cells were biomechanically integrated to act like a syncytium as exists in native ASM tissue. This may suggest that microtissues better replicate native tissue than traditional 2D cell culture techniques. The notable exception to strain homogeneity was following cytochalasin D, where the greatest strain changes were localized to the areas closest to the cantilevers. Although it is possible that drug diffusion or cell permeability was higher in these areas, the relaxation pattern is more likely related to how tension was transferred from the microtissue to the cantilevers. Specifically, the areas of fastest relaxation were the same areas where the actin stress fibers that encircled the cantilevers began radiating inward toward the center of the microtissue. These localized areas would be under the greatest stress and thus would be expected to exhibit higher strain rates when the actin cytoskeleton was compromised.

Results from the 10-min drug exposures demonstrated that ASM-3T3 microtissues were capable of significant force generation above baseline levels. Since the maximal histamine and acetylcholine responses were significantly lower than for KCl it suggests that contraction may be limited by reduced M_3 and H_1 receptor expression or phospholipase C coupling, consistent with observations in traditional 2D cell cultures (16, 63). Although we did expect some similarities between microtissue and OMTC measurements of cell contraction, the degree to which normalized acetylcholine and KCl responses harmonized was not anticipated. However, the stark contrast observed between histamine responses in the two models was equally surprising. This histamine data were compiled from 31 individual microtissues and 14 petri dishes of 2D cells performed in conjunction with other contractile agonists and thus was highly reproducible. However, our 2D histamine results do differ from a previous study in which contraction to 10 μM histamine was only marginally higher than the response to 50 mM KCl (34). This may suggest that the high 2D response to histamine we have observed is a feature of the particular immortalized human ASM cell line used in our experiments. Nevertheless, this same cell line was used in both the 2D and 3D cultures, indicating a potent effect from the 3D architecture.

The disparity between our 2D and 3D cultures may be due to several factors including differences in H_1 receptor expression or sensitivity, additional effects of H_2 and H_4 receptors, and downstream factors including histamine modulation of the actin cytoskeleton (48).

Further disparity between 2D and 3D cultures is evident from the stronger relaxation response to forskolin and cytochalasin D in ASM-3T3 microtissues. Since forskolin relaxes ASM by increasing cAMP, reducing both inositol triphosphate-mediated calcium release from the sarcoplasmic reticulum (5) and calcium sensitivity (6), it is unclear whether resting cytoplasmic calcium levels are high or calcium sensitivity was elevated in microtissues. The use of alternative relaxant factors that operate downstream from cAMP and calcium, including the ROCK inhibitor Y27632 and the MYLK inhibitor ML7, would help elucidate the mechanism responsible for the high baseline tone. In any case, our results indicate that there was a high level of active tension attributable to actinomyosin cross-bridge cycling even at baseline, as well as significant passive cytoskeletal stiffness. Similar intrinsic ASM tone has been observed under many circumstances including ex vivo human airway segments (46, 51) and in 2D cultures (2, 34). This may provide a benefit for microtissues over ex vivo ASM strips, which tend to have far less active tension than airway segments (37) and do not show relaxation responses unless previously activated with a contractile agonist.

Despite the similarities demonstrated in normalized comparisons of contractile function, direct comparison of our two models by gene expression analysis suggests that the 3D geometry in ASM-3T3 microtissues was promoting elevated contractile function relative to traditional 2D cells. Specifically, ASM-3T3 microtissues exhibited significantly higher abundance of MHC and MYLK mRNAs than 2D cells, whereas MYPT1 appeared to be unregulated by substrate geometry. However, the mechanisms underpinning these gene expression changes are unclear because of differential regulation of key transcription factors; SRF was downregulated in microtissues whereas MYOCD was upregulated. We cannot currently discount the possibility of differences in mRNA stability between the two models, or the possibility that changes in mRNA abundance do not translate to changes in abundance of key contractile proteins, which may warrant further study.

When considering our gene expression analysis, it is also important to note that ASM-3T3 microtissues exhibited significantly lower mRNA abundance of three candidate housekeeping controls. Some of this difference can be explained by the fact that a small portion of the total RNA content of microtissues was contributed by mouse 3T3 fibroblasts and thus was not amplified by our human-specific qPCR primers. However, 3T3 fibroblasts only constituted 20% of the initial cell complement and did not appear to increase in number over time (see Figs. 2 and 3*D*). It is not unexpected that "traditional" housekeeping controls would be dissimilar between these dif-

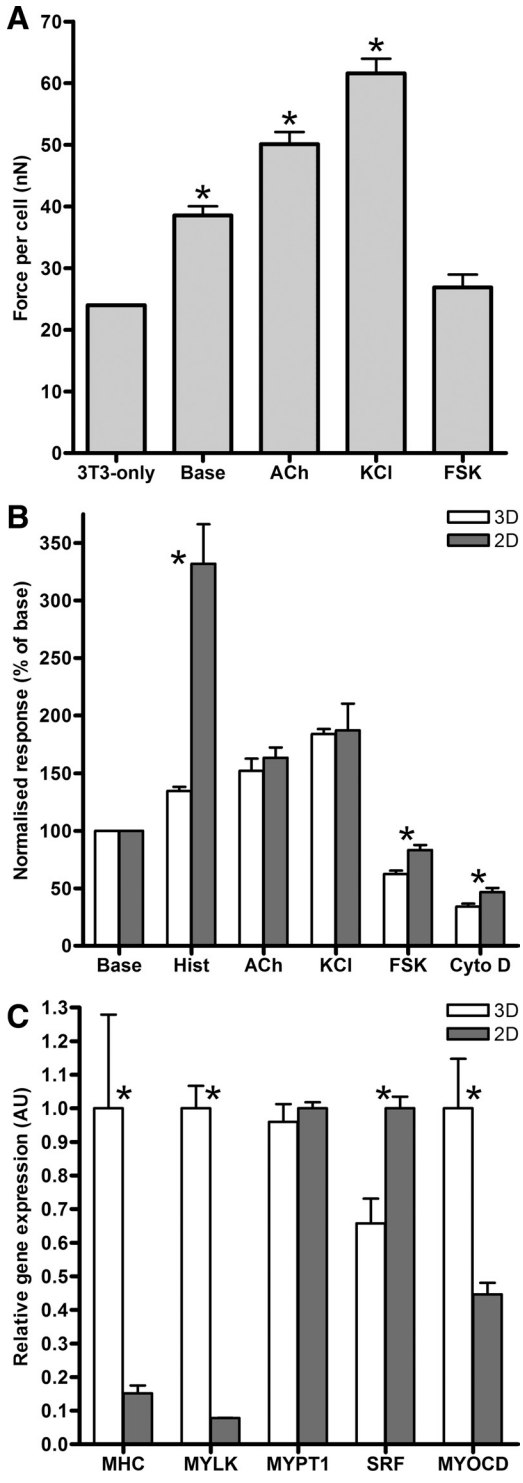

Fig. 7. In vitro model comparisons. *A*: ASM-3T3 microtissues ($n \geq 16$) generated more baseline force per cell than 3T3 fibroblasts produced with the same substrates (41), and even more tension when contraction to acetylcholine and KCl are considered (*t*-test $P < 0.0001$). Relaxation to FSK, representing ASM cells without contractile tone, generates equivalent tension per cell to 3T3 cells alone (*t*-test $P = 0.1791$). *B*: comparing 3D microtissues ($n \geq 31$) to ASM cells in 2D measured with optical magnetic twisting cytometry (OMTC) ($n \geq 11$), acetylcholine and KCl responses are virtually identical, whereas histamine is vastly different; 2D cells exhibit much stronger contractions. 3D microtissues also relaxed significantly more to both FSK and Cyto D. *C*: gene expression analysis of 3D microtissues and 2D cells ($n = 4$) demonstrates that microtissues had significantly higher levels of MHC, MYLK, and MYOCD (*t*-test $P \leq 0.0233$), whereas SRF was significantly lower (*t*-test $P = 0.0056$) and MYPT1 exhibited no change (*t*-test $P = 0.4973$). *Significant difference from 3T3-only (*A*) or between 2D and 3D cultures (*B* and *C*).

Table 3. *Selection of a housekeeping control for gene expression analysis*

	YWHAZ		UBC		GAPDH	
	3D	2D	3D	2D	3D	2D
Ct	21.92 ± 0.13	19.87 ± 0.05	29.84 ± 0.05	27.99 ± 0.04	18.46 ± 0.05	16.92 ± 0.02
$E^{\Delta Ct}$	1.22 ± 0.10	4.43 ± 0.13	1.03 ± 0.04	3.49 ± 0.08	1.07 ± 0.04	3.03 ± 0.04
Bestkeeper Pearson correlation coefficient	0.997		0.998		0.996	
Bestkeeper *P* value	0.001		0.001		0.001	
NormFinder stability value	0.437		0.077		0.381	

Candidate housekeeping controls displayed very strong consistency of expression within each culture type, but all three exhibited significantly higher expression in 2D cultures. Analysis of pooled data by use of Bestkeeper and NormFinder demonstrate that UBC was the most stably expressed candidate, thus this gene was used as the reference for ΔΔCt calculations.

ferent experimental models, but the large magnitude of the difference strongly indicates that mRNA in microtissues comprises a smaller proportion of the total cellular RNA. This observation may agree with other studies that demonstrate key cellular functions unrelated to contraction can be regulated by the 3D substrate geometry (14, 56).

To further validate ASM-3T3 microtissues as a model of ASM contraction we also determined two directly comparable metrics, namely force per cell and tissue stress. As expected, ASM-3T3 microtissues reported a higher average force per cell than 3T3 cells alone found in a previous study (41). As described above, this can be attributed to the presence of active contractile tone in addition to passive cytoskeletal tension at baseline. However, the close matching of force per cell from forskolin-treated ASM-3T3 microtissues vs. 3T3-alone microtissues was surprising. This suggests that the core biomechanical properties of these two mesenchymal-origin cells from different species are remarkably similar, although considering that we demonstrate differences in baseline and contracted tension between immortalized and primary ASM cells, this metric may be highly dependent on the source cells.

When comparing cross-sectional stress of contracted microtissues to ex vivo ASM strips, the significantly lower stresses developed by microtissues were not unexpected. Microtissue force production is measured as a direct result of ASM shortening against an auxotonic load, which includes some tissue shortening as the cantilevers bend. Thus our model lies between isometric and isotonic contraction, and force production will be lower than the potential isometric maximum (57). Perhaps more significant is that cultured ASM cells in vitro have substantially less contractile protein content compared with ex vivo ASM (28). Although contractile protein content was not assessed in our study, our lower stress results indicate that 3D culture alone is incapable of restoring contractile protein content of in vitro cells to levels comparable to native tissues, and microtissues still present this same limitation of other cultured cell models.

Given that recapitulating a highly contractile phenotype in ASM cells can be mediated by the ECM (58), and collagen has been shown to negatively regulate contractile protein expression (32), it is possible that a more physiological mix of ECM components that includes laminin may be able to increase contractile function. In this context, it would also be valuable to compare the contractile phenotype and function of microtissues to decellularized ASM matrixes repopulated with cultured cells and native ex vivo ASM strips. Although not possible with the current iteration of microfabricated tissue gauges, it may also be important to determine whether applying dynamic mechanical strain alters the contractility of ASM in 3D microtissues. In traditional 2D cultures of ASM, dynamic mechanical strain can have potent effects, acutely eliciting cytoskeletal fluidization (40) and depending on the exact nature of the strain regime it can elicit chronic changes in ASM phenotype and function (22, 44), but it is currently unclear whether 3D cell geometry may alter these responses.

Microtissues as a flexible multicell model. ASM microtissues required supplementation with 3T3 fibroblasts, since this markedly improved the number of successful tissues and survival times, without exhibiting many complications seen with growing two different cell types together in traditional 2D cell cultures. This finding is reminiscent of tissue engineered cardiac muscle constructs in which the inclusion of fibroblasts is absolutely critical for normal contractile function. In the absence of fibroblasts, cardiac muscle cells exhibit poor tissue remodeling and low cellular alignment (49); gap junction protein expression and synchronization of spontaneous contractions are also reduced (49), presumably because of inappropriate ECM signaling. However, it is important to note that fibroblasts were important only for the structural integrity of ASM, but not contractile function, since ASM-only microtissues did generate baseline tension and contract to KCl (data not shown). In this context, the exact cause of microtissue failure and the mechanism by which fibroblasts improved microtissue integrity are unclear since there were also no apparent differences in gross morphology. Although it is possible that there was a reduction in overall tension because of the inclusion of noncontractile cells, this seems an unlikely source of improvement since microtissues predominantly failed at baseline, and failure was never observed in any experiment despite the very large tensions that were generated during KCl contractions. Thus it seems likely that the higher ECM secretion by fibroblasts compared with contractile ASM cells augmented and reinforced the ECM in which the cells were initially seeded. Indeed, 3T3 microtissues were shown to actively produce ECM as evidenced by the production of fibronectin and tenascin D (41).

The presence of multiple cell types creates a more complex model and may complicate data analysis where purely ASM behavior is being studied. However, by including fibroblasts the model more closely mimics the ASM layer in vivo, which does contain fibroblasts, and thus may make ASM-3T3 microtissues useful for studying many respiratory diseases that feature pathological fibroblast function including hyperplasia, chemotaxis to and within the airway wall, or inappropriate differentiation to myofibroblasts (30). In addition to the 3T3 fibroblasts used to develop the model, we also produced ASM

microtissues with the more physiologically relevant WI-38 human lung fibroblast cell line, as well as primary human ASM cells sourced from lung explants (passage ≤4). The success of these tissues suggests a great degree of flexibility for selecting cells with certain characteristics or genetic modifications, with some caveats. Primary cells exhibited significantly higher baseline and contracted tension values than immortalized cells, such that several measurements exceeded the accurate/linear capability of the cantilevers. As such, stiffer cantilevers will need to be used in future studies where increases in contractile protein content are expected, which can be achieved by increasing cantilever thickness and using PDMS with a higher elastic modulus.

It is important to note that when using primary ASM cells we saw no difference in contractile responses between microtissues using 3T3 and WI-38 fibroblasts. This may indicate that key features of these two fibroblast types such as ECM production, cytokine secretion, or gap junction formation exert similar (or no) effect on ASM contractile function, or that extracellular signaling is dominated by the collagen I matrix in which the cells are initially seeded. Nevertheless, the flexibility of fibroblast content combined with the ability of the cells to remodel the ECM suggests that ASM microtissues may be more useful than ex vivo tissue for studying ECM remodeling processes and how these relate to ASM function. There may also be significant potential for microtissues to work as a multicell model with other airway cell types related to remodeling such as inflammatory cells or airway epithelium where physical contact between cells in a physiologically relevant 3D environment may be important. For example, there is strong evidence that ASM interacts with T cells directly through cell-surface antigens resulting in the release of IL-13 (59), whereas existing coculture and conditioned medium systems are only capable of assessing the effects of soluble mediators.

Tissue engineering considerations: microtissue formation, longevity, and cell proliferation. It is important to note that many other alternative approaches were attempted to improve the success rates and longevity of ASM-only tissues, which are useful to bring to light considering the future potential of tissue engineering techniques to replace damaged lung tissue (54). Because the principal mode of failure was tissues dissociating from the cantilevers, which may have been due to tension development during formation, we attempted to reduce contractile tone by treatment with the long-acting β_2-agonist formoterol, but this provided no benefit to microtissue longevity. Since ASM cells secrete a range of matrix metalloproteinases (MMPs) that can degrade collagen, particularly MMP-1, -2, -3 and -9 (20), we also incubated some microtissues with the broad-spectrum MMP inhibitor minocycline after fabrication. However, this treatment prevented microtissue compaction and tissues did not form, suggesting that MMP activity is integral to ECM remodeling. Higher collagen concentrations were also used in an effort to increase matrix integrity, but the increased viscosity of collagen solutions (>3 mg/ml) made it exceedingly difficult to degas the wells and to centrifuge cells into the wells. Finally, increasing the D-ribose concentration beyond 15 mM to further cross-link the collagen matrix (24) also provided no additional benefit. It may be possible to stimulate ASM to secrete ECM with transforming growth factor β (TGF-β) and connective tissue growth factor (CTGF) (36) or ascorbic acid (15). However, this approach would produce off-target phenotypic effects, and their routine use as a core component of the methodology would preclude their use as experimental treatments. TGF-β in particular increases the transcription of ASM-specific genes (29, 62) and elevated levels of TGF-β are strongly implicated in the pathogenesis of asthma (43).

Nevertheless, since ASM-3T3 microtissues eventually dissociated from the cantilevers via the same mechanism as those made with ASM alone, there are likely further methodological optimizations that could improve structural integrity. Despite the presumed ECM protein secretion from fibroblasts, the structure is still comprised largely of collagen I, which is subject to degradation from MMP-1, -2, -3, and -9, and this degradation may ultimately play a key role in microtissue failure. The inclusion of an additional structural protein that is more resistant to degradation by these specific MMPs could provide additional structural integrity, namely fibrin, which has been used successfully in cardiac microtissues (11).

It is also important to consider that cell proliferation could negatively affect microtissue structure. Parent cells must partially detach from the substrate during mitosis, resulting in tension loss, and the absence of a physical barrier at the tissue borders makes it unlikely that the daughter cells would consistently re-integrate correctly into the microtissue. Whether this is a factor in long-term survival is unclear; ASM-3T3 microtissues never visibly increased in size during the first 4 days, indicating that the basal proliferation rate in young microtissues was very low. This is despite the fact that these cells, which have a doubling time <48 h in traditional 2D cultures, are in a very pro-proliferative environment with high serum (31) and a collagen I matrix (32). Thus it appears that the 3D substrate geometry was exerting inhibitory effects on ASM proliferation, which is consistent with previous studies on 3D smooth muscle cultures (14, 56). Notwithstanding inhibitory effects on proliferation, we observed that high-serum medium was critical for microtissue formation because reducing serum levels to 1% immediately after fabrication prevented the cells from compacting and remodeling the gel into a microtissue. This may be due to a lack of soluble factors required for ECM remodeling and cell motility or could be due to increased adherence to the sides of the PDMS wells, but the exact cause is currently unclear. Reducing serum concentrations only after gel compaction and remodeling has completed (6–24 h) may help to improve long-term microtissue survival and could be a feasible strategy for allowing this model to study cell-cycle regulation. It will also be important to assess the effects of serum on contractile phenotype in 3D considering the potent serum effects observed in traditional 2D cultures (27).

Summary. ASM-3T3 microtissues represent a physiologically relevant tissue engineered model of ASM contraction. Benefits include that microtissues compact and remodel the matrix into a highly organized and dense 3D structure that generates substantial baseline tension. Critically, ASM-3T3 microtissues responded appropriately to a selection of key contractile and relaxant agents, indicating viability and suitability of the model to study ASM contractile function. The high throughput capabilities and low resource requirements of this model make it attractive as an improvement on traditional 2D cell culture for routine study because of the physiologically relevant mechanical environment. Furthermore, microtissues

could possibly be a legitimate alternative to ex vivo ASM strips, particularly when studying the effects of airway wall remodeling on ASM function or mechanisms governing intrinsic ASM tone. Future experiments involving manipulation of the biochemical and mechanical environment, and creating microtissues with additional cell types or genetically modified cells, could be employed to study how these factors contribute to the pathogenesis of asthma.

GRANTS

This study was funded by Canadian Institutes of Health Research, Postdoctoral Fellowship (A. West); Canadian Institutes of Health Research, Operating Grant; Lung Association of Nova Scotia, Legacy Research Fund Grant; and Nova Scotia Health Research Foundation, Research Capacity Award. The grant bodies had no role in study design, data collection and analysis, decision to publish, or preparation of the manuscript.

DISCLOSURES

No conflicts of interest, financial or otherwise, are declared by the author(s).

AUTHOR CONTRIBUTIONS

A.R.W., W.R.L., T.B., C.S.C., E.A.C., and G.N.M. conception and design of research; A.R.W., N.Z., D.J.C., and M.J.W. performed experiments; A.R.W., N.Z., J.T.F., and G.R.G. analyzed data; A.R.W. and G.N.M. interpreted results of experiments; A.R.W., J.T.F., and G.R.G. prepared figures; A.R.W. drafted manuscript; A.R.W., E.A.C., and G.N.M. edited and revised manuscript; A.R.W., N.Z., D.J.C., M.J.W., W.R.L., T.B., C.S.C., J.T.F., G.R.G., E.A.C., and G.N.M. approved final version of manuscript.

REFERENCES

1. **An SS, Kim J, Ahn K, Trepat X, Drake KJ, Kumar S, Ling G, Purington C, Rangasamy T, Kensler TW, Mitzner W, Fredberg JJ, Biswal S.** Cell stiffness, contractile stress and the role of extracellular matrix. *Biochem Biophys Res Commun* 382: 697–703, 2009.
2. **An SS, Laudadio RE, Lai J, Rogers RA, Fredberg JJ.** Stiffness changes in cultured airway smooth muscle cells. *Am J Physiol Cell Physiol* 283: C792–C801, 2002.
3. **Andersen CL, Jensen JL, Orntoft TF.** Normalization of real-time quantitative reverse transcription-PCR data: a model-based variance estimation approach to identify genes suited for normalization, applied to bladder and colon cancer data sets. *Cancer Res* 64: 5245–5250, 2004.
4. **Araujo BB, Dolhnikoff M, Silva LF, Elliot J, Lindeman JH, Ferreira DS, Mulder A, Gomes HA, Fernezlian SM, James A, Mauad T.** Extracellular matrix components and regulators in the airway smooth muscle in asthma. *Eur Respir J* 32: 61–69, 2008.
5. **Bai Y, Sanderson MJ.** Airway smooth muscle relaxation results from a reduction in the frequency of Ca^{2+} oscillations induced by a cAMP-mediated inhibition of the IP_3 receptor. *Respir Res* 7: 34, 2006.
6. **Bai Y, Sanderson MJ.** Modulation of the Ca^{2+} sensitivity of airway smooth muscle cells in murine lung slices. *Am J Physiol Lung Cell Mol Physiol* 291: L208–L221, 2006.
7. **Baldwin L, Roche WR.** Does remodelling of the airway wall precede asthma? *Paediatr Respir Rev* 3: 315–320, 2002.
8. **Balestrini JL, Skorinko JK, Hera A, Gaudette GR, Billiar KL.** Applying controlled non-uniform deformation for in vitro studies of cell mechanobiology. *Biomech Model Mechanobiol* 9: 329–344, 2010.
9. **Barnes PJ.** Immunology of asthma and chronic obstructive pulmonary disease. *Nat Rev Immunol* 8: 183–192, 2008.
10. **Blanc FX, Coirault C, Salmeron S, Chemla D, Lecarpentier Y.** Mechanics and crossbridge kinetics of tracheal smooth muscle in two inbred rat strains. *Eur Respir J* 22: 227–234, 2003.
11. **Boudou T, Legant WR, Mu A, Borochin MA, Thavandiran N, Radisic M, Zandstra PW, Epstein JA, Margulies KB, Chen CS.** A microfabricated platform to measure and manipulate the mechanics of engineered cardiac microtissues. *Tissue Eng Part A* 18: 910–919, 2012.
12. **Bramley AM, Roberts CR, Schellenberg RR.** Collagenase increases shortening of human bronchial smooth muscle in vitro. *Am J Respir Crit Care Med* 152: 1513–1517, 1995.
13. **Bramley AM, Thomson RJ, Roberts CR, Schellenberg RR.** Hypothesis: excessive bronchoconstriction in asthma is due to decreased airway elastance. *Eur Respir J* 7: 337–341, 1994.
14. **Ceresa CC, Knox AJ, Johnson SR.** Use of a three-dimensional cell culture model to study airway smooth muscle-mast cell interactions in airway remodeling. *Am J Physiol Lung Cell Mol Physiol* 296: L1059–L1066, 2009.
15. **Choi KM, Seo YK, Yoon HH, Song KY, Kwon SY, Lee HS, Park JK.** Effect of ascorbic acid on bone marrow-derived mesenchymal stem cell proliferation and differentiation. *J Biosci Bioeng* 105: 586–594, 2008.
16. **Daykin K, Widdop S, Hall IP.** Control of histamine induced inositol phospholipid hydrolysis in cultured human tracheal smooth muscle cells. *Eur J Pharmacol* 246: 135–140, 1993.
17. **Dekkers BG, Schaafsma D, Nelemans SA, Zaagsma J, Meurs H.** Extracellular matrix proteins differentially regulate airway smooth muscle phenotype and function. *Am J Physiol Lung Cell Mol Physiol* 292: L1405–L1413, 2007.
18. **Deng L, Fairbank NJ, Fabry B, Smith PG, Maksym GN.** Localized mechanical stress induces time-dependent actin cytoskeletal remodeling and stiffening in cultured airway smooth muscle cells. *Am J Physiol Cell Physiol* 287: C440–C448, 2004.
19. **Dolhnikoff M, da Silva LF, de Araujo BB, Gomes HA, Fernezlian S, Mulder A, Lindeman JH, Mauad T.** The outer wall of small airways is a major site of remodeling in fatal asthma. *J Allergy Clin Immunol* 123: 1090–1097, 1097.e1, 2009.
20. **Elshaw SR, Henderson N, Knox AJ, Watson SA, Buttle DJ, Johnson SR.** Matrix metalloproteinase expression and activity in human airway smooth muscle cells. *Br J Pharmacol* 142: 1318–1324, 2004.
21. **Fabry B, Maksym GN, Shore SA, Moore PE, Panettieri RA Jr, Butler JP, Fredberg JJ.** Selected contribution: time course and heterogeneity of contractile responses in cultured human airway smooth muscle cells. *J Appl Physiol* 91: 986–994, 2001.
22. **Fairbank NJ, Connolly SC, Mackinnon JD, Wehry K, Deng L, Maksym GN.** Airway smooth muscle cell tone amplifies contractile function in the presence of chronic cyclic strain. *Am J Physiol Lung Cell Mol Physiol* 295: L479–L488, 2008.
23. **Gillis JM, Cao ML, Godfraind-De Becker A.** Density of myosin filaments in the rat anococcygeus muscle, at rest and in contraction. II. *J Muscle Res Cell Motil* 9: 18–29, 1988.
24. **Girton TS, Oegema TR, Tranquillo RT.** Exploiting glycation to stiffen and strengthen tissue equivalents for tissue engineering. *J Biomed Mater Res* 46: 87–92, 1999.
25. **Gosens R, Stelmack GL, Dueck G, McNeill KD, Yamasaki A, Gerthoffer WT, Unruh H, Gounni AS, Zaagsma J, Halayko AJ.** Role of caveolin-1 in p42/p44 MAP kinase activation and proliferation of human airway smooth muscle. *Am J Physiol Lung Cell Mol Physiol* 291: L523–L534, 2006.
26. **Griffith LG, Swartz MA.** Capturing complex 3D tissue physiology in vitro. *Nat Rev Mol Cell Biol* 7: 211–224, 2006.
27. **Halayko AJ, Camoretti-Mercado B, Forsythe SM, Vieira JE, Mitchell RW, Wylam ME, Hershenson MB, Solway J.** Divergent differentiation paths in airway smooth muscle culture: induction of functionally contractile myocytes. *Am J Physiol Lung Cell Mol Physiol* 276: L197–L206, 1999.
28. **Halayko AJ, Salari H, Ma X, Stephens NL.** Markers of airway smooth muscle cell phenotype. *Am J Physiol Lung Cell Mol Physiol* 270: L1040–L1051, 1996.
29. **Hinson JS, Medlin MD, Lockman K, Taylor JM, Mack CP.** Smooth muscle cell-specific transcription is regulated by nuclear localization of the myocardin-related transcription factors. *Am J Physiol Heart Circ Physiol* 292: H1170–H1180, 2007.
30. **Hinz B, Phan SH, Thannickal VJ, Galli A, Bochaton-Piallat ML, Gabbiani G.** The myofibroblast: one function, multiple origins. *Am J Pathol* 170: 1807–1816, 2007.
31. **Hirst SJ, Barnes PJ, Twort CH.** Quantifying proliferation of cultured human and rabbit airway smooth muscle cells in response to serum and platelet-derived growth factor. *Am J Respir Cell Mol Biol* 7: 574–581, 1992.
32. **Hirst SJ, Twort CH, Lee TH.** Differential effects of extracellular matrix proteins on human airway smooth muscle cell proliferation and phenotype. *Am J Respir Cell Mol Biol* 23: 335–344, 2000.
33. **Holgate ST.** Epithelium dysfunction in asthma. *J Allergy Clin Immunol* 120: 1233–1244; quiz 1245–1236, 2007.

34. **Hubmayr RD, Shore SA, Fredberg JJ, Planus E, Panettieri RA Jr, Moller W, Heyder J, Wang N.** Pharmacological activation changes stiffness of cultured human airway smooth muscle cells. *Am J Physiol Cell Physiol* 271: C1660–C1668, 1996.
35. **Jiang H, Halayko AJ, Rao K, Cunningham P, Stephens NL.** Normalization of force generated by canine airway smooth muscles. *Am J Physiol Lung Cell Mol Physiol* 260: L522–L529, 1991.
36. **Johnson PR, Burgess JK, Ge Q, Poniris M, Boustany S, Twigg SM, Black JL.** Connective tissue growth factor induces extracellular matrix in asthmatic airway smooth muscle. *Am J Respir Crit Care Med* 173: 32–41, 2006.
37. **Jongejan RC, de Jongste JC, van Strik R, Raatgeep HR, Bonta IL, Kerrebijn KF.** Measurement of human small airway smooth muscle function in vitro. Comparison of bronchiolar strips and segments. *J Pharmacol Methods* 20: 135–142, 1988.
38. **Kelly DJ, Azeloglu EU, Kochupura PV, Sharma GS, Gaudette GR.** Accuracy and reproducibility of a subpixel extended phase correlation method to determine micron level displacements in the heart. *Med Eng Phys* 29: 154–162, 2007.
39. **Khan MA, Ellis R, Inman MD, Bates JH, Sanderson MJ, Janssen LJ.** Influence of airway wall stiffness and parenchymal tethering on the dynamics of bronchoconstriction. *Am J Physiol Lung Cell Mol Physiol* 299: L98–L108, 2010.
40. **Krishnan R, Park CY, Lin YC, Mead J, Jaspers RT, Trepat X, Lenormand G, Tambe D, Smolensky AV, Knoll AH, Butler JP, Fredberg JJ.** Reinforcement versus fluidization in cytoskeletal mechanoresponsiveness. *PloS One* 4: e5486, 2009.
41. **Legant WR, Pathak A, Yang MT, Deshpande VS, McMeeking RM, Chen CS.** Microfabricated tissue gauges to measure and manipulate forces from 3D microtissues. *Proc Natl Acad Sci USA* 106: 10097–10102, 2009.
42. **Long X, Bell RD, Gerthoffer WT, Zlokovic BV, Miano JM.** Myocardin is sufficient for a smooth muscle-like contractile phenotype. *Arterioscler Thromb Vasc Biol* 28: 1505–1510, 2008.
43. **Makinde T, Murphy RF, Agrawal DK.** The regulatory role of TGF-beta in airway remodeling in asthma. *Immunol Cell Biol* 85: 348–356, 2007.
44. **Maksym GN, Deng L, Fairbank NJ, Lall CA, Connolly SC.** Beneficial and harmful effects of oscillatory mechanical strain on airway smooth muscle. *Can J Physiol Pharmacol* 83: 913–922, 2005.
45. **Matsumoto H, Moir LM, Oliver BG, Burgess JK, Roth M, Black JL, McParland BE.** Comparison of gel contraction mediated by airway smooth muscle cells from patients with and without asthma. *Thorax* 62: 848–854, 2007.
46. **McParland BE, Pare PD, Johnson PR, Armour CL, Black JL.** Airway basement membrane perimeter in human airways is not a constant; potential implications for airway remodeling in asthma. *J Appl Physiol* 97: 556–563, 2004.
47. **Miller C, George S, Niklason L.** Developing a tissue-engineered model of the human bronchiole. *J Tissue Eng Regen Med* 4: 619–627, 2010.
48. **Mitsuhashi M, Payan DG.** Characterization of functional histamine H1 receptors on a cultured smooth muscle cell line. *J Cell Physiol* 134: 367–375, 1988.
49. **Nichol JW, Engelmayr GC Jr, Cheng M, Freed LE.** Co-culture induces alignment in engineered cardiac constructs via MMP-2 expression. *Biochem Biophys Res Commun* 373: 360–365, 2008.
51. **Noble PB, Jones RL, Needi ET, Cairncross A, Mitchell HW, James AL, McFawn PK.** Responsiveness of the human airway in vitro during deep inspiration and tidal oscillation. *J Appl Physiol* 110: 1510–1518, 2011.
52. **Pare PD, McParland BE, Seow CY.** Structural basis for exaggerated airway narrowing. *Can J Physiol Pharmacol* 85: 653–658, 2007.
53. **Pfaffl MW, Tichopad A, Prgomet C, Neuvians TP.** Determination of stable housekeeping genes, differentially regulated target genes and sample integrity: BestKeeper–Excel-based tool using pair-wise correlations. *Biotechnol Lett* 26: 509–515, 2004.
54. **Prakash YS, Stenmark KR.** Bioengineering the lung: molecules, materials, matrix, morphology, and mechanics. *Am J Physiol Lung Cell Mol Physiol* 302: L361–L362, 2012.
55. **Small JV, Celis JE.** Filament arrangements in negatively stained cultured cells: the organization of actin. *Cytobiologie* 16: 308–325, 1978.
56. **Song J, Rolfe BE, Hayward IP, Campbell GR, Campbell JH.** Effects of collagen gel configuration on behavior of vascular smooth muscle cells in vitro: association with vascular morphogenesis. *In Vitro Cell Devel Biol Anim* 36: 600–610, 2000.
57. **Stephens NL, Van Niekerk W.** Isometric and isotonic contractions in airway smooth muscle. *Can J Physiol Pharmacol* 55: 833–838, 1977.
58. **Tran T, Ens-Blackie K, Rector ES, Stelmack GL, McNeill KD, Tarone G, Gerthoffer WT, Unruh H, Halayko AJ.** Laminin-binding integrin alpha7 is required for contractile phenotype expression by human airway myocytes. *Am J Respir Cell Mol Biol* 37: 668–680, 2007.
59. **Veler H, Hu A, Fatma S, Grunstein JS, DeStephan CM, Campbell D, Orange JS, Grunstein MM.** Superantigen presentation by airway smooth muscle to CD4+ T lymphocytes elicits reciprocal proasthmatic changes in airway function. *J Immunol* 178: 3627–3636, 2007.
60. **Wang N, Tolic-Norrelykke IM, Chen J, Mijailovich SM, Butler JP, Fredberg JJ, Stamenovic D.** Cell prestress. I. Stiffness and prestress are closely associated in adherent contractile cells. *Am J Physiol Cell Physiol* 282: C606–C616, 2002.
61. **West AR, Oates PS.** Decreased sucrase and lactase activity in iron deficiency is accompanied by reduced gene expression and upregulation of the transcriptional repressor PDX-1. *Am J Physiol Gastrointest Liver Physiol* 289: G1108–G1114, 2005.
62. **Wicks J, Haitchi HM, Holgate ST, Davies DE, Powell RM.** Enhanced upregulation of smooth muscle related transcripts by TGF beta2 in asthmatic (myo) fibroblasts. *Thorax* 61: 313–319, 2006.
63. **Widdop S, Daykin K, Hall IP.** Expression of muscarinic M2 receptors in cultured human airway smooth muscle cells. *Am J Respir Cell Mol Biol* 9: 541–546, 1993.